Langmuir

ARTICLE

pubs.acs.org/Langmuir

# Analysis of Affinity Maps of Membrane Proteins on Individual Human Embryonic Stem Cells

Zhaoxia Li,[†] Dengli Qiu,[†] Kangmin Xu,[‡] Indumathi Sridharan,[†] Xiaoping Qian,[‡] and Rong Wang*[,†]

[†]Department of Biological, Chemical and Physical Sciences, and [‡]Department of Mechanical, Materials, and Aerospace Engineering, Illinois Institute of Technology, Chicago, Illinois 60616, United States

Supporting Information

**ABSTRACT:** The heterogeneity found in many cell types has greatly inspired research in single-cell gene and protein profiling for discovering the origin of heterogeneity and its role in cell fate decisions. Among the existing techniques to probe heterogeneity, atomic force microscopy (AFM) utilizes an antibody/ligand-modified tip to explore the distribution of a target membrane protein on individual cells in their native environment. In this paper, we establish a practical model to analyze the data systematically, and attempt the quantification of membrane protein abundance on single cells by taking account issues, such as the level of nonspecific interaction, the probe resolution, and the reproducibility of detecting protein distribution. We demonstrated the application in examining the heterogeneous distribution and the local protein abundance of TRA-1-81 antigen on human embryonic stem (hES) cells at the subcellular level. Heterogeneity in TRA-1-81 expression was also detected at the single cell level, suggesting the presence of subpopulation cells within an undifferentiated hES cell colony. The method provides a platform to unveiling the correlation between heterogeneity of membrane proteins and cell development in a complex cell community.

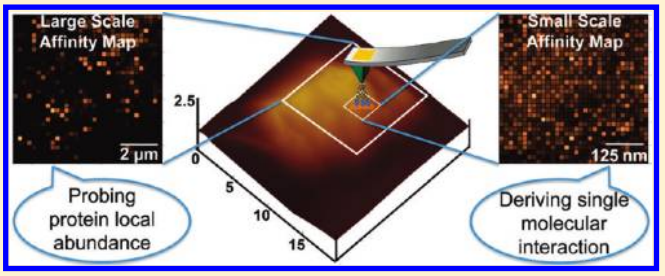


## INTRODUCTION

With the recent advancement in single-cell analytical techniques, transcriptional and temporal heterogeneity has been found in many cell types, including human embryonic stem (hES) cells. Stem cells grown in vivo or in vitro are exposed to the surrounding niche cells, the extracellular matrix, and various soluble stimuli. These factors coax the stem cells to proliferate or differentiate by balancing the number of quiescent and cycling stem cells within the original stem cell colony.[1−4] Thus, individual cells behave differently in response to inductive cues; subpopulation cells present in a single stem cell colony and the coordination among cells in different subpopulations govern the cell fate decision.[5,6] Optimization of protocols for generating clinically relevant cell types largely relies on the information derived from identified individual cells and not on the basis of population-scale cell analysis as in classical approaches.[4] Current single-cell profiling techniques include live cell imaging,[7,8] fluorescence-activated cell sorting (FACS),[9,10] single-cell microfluidic processing,[11−14] MS2 systematic analysis,[15] laser capture microdissection (LCM),[16,17] patch-clamp aspiration,[18,19] micropipetting,[20] etc.

Complementary to these techniques, mapping of cell membrane proteins by atomic force microscopy (AFM) provides an alternative approach for examining proteins on cells in their native growth environment at a high spatial resolution.[21−24] Among various AFM modes, single-molecule force spectroscopy can be applied to the study of membrane proteins in cells by visualizing the individual proteins[25] and counting the protein numbers.[26,27] This application has been mainly demonstrated on simple substrates, such as purified proteins or isolated cytoplasmic membranes containing dense and highly ordered protein arrays on glass or mica. A cell membrane is rough, soft, and complex due to the diverse distribution of various cell-surface proteins and phospholipids. Hence, studies on cells are more challenging than those on simplified substrates.

Affinity mapping utilizes an antibody (or ligand)-modified AFM tip to discriminate a target membrane protein from other species via force measurement regardless of cell surface roughness. When the tip scans on a cell membrane, it reports the target membrane protein selectively and reveals its distribution, association, and local abundance of the protein at the subcellular level. This method is superior to many other imaging approaches, e.g., immunohistochemistry, electron microscopy, and fluorescent molecular- or particle-based imaging tools. These approaches can provide the relative quantification of proteins and are not precise for analyzing low-abundance proteins because of the intrinsic limitations of diffusion-controlled processes and the background signal.

Although the affinity mapping method also relies on the interactions between antigen−antibody or ligand−receptor, due to the direct "touch" approach, the local concentration of antibody or ligand is sufficiently high. This warrants the specific interaction

**Received:** March 3, 2011
**Revised:** April 26, 2011
**Published:** June 09, 2011

between the counter proteins on the tip and on the cell membrane and consequently the absolute quantification of both high and low abundant proteins. Artifacts have to be eliminated during data acquisition and analysis. For instance, the level of nonspecific interaction should be determined, the collection of affinity maps must warrant the reproducibility, and the evaluation of probe resolution is essential to achieve meaningful protein distribution information. With the analysis of membrane protein TRA-1-81 antigen on the surface of hES cells, we attempt to address these issues in the current study to establish a global quantitative method in probing membrane proteins on cells in their native states. Heterogeneity in TRA-1-81 expression was revealed at both the subcellular level and the cell colony level.

## MATERIALS AND METHODS

**hES Cell Culture.** Human embryonic stem cell line H9 was from WiCell (Madison, WI). Cells were routinely cultured on feeder cells derived from mitotically inactivated mouse embryo fibroblast (MEFs). Cells were maintained in DMEM/F12 (Mediatech, Herndon, VA), containing 20% knockout serum replacement, 1% nonessential amino acid, 1 mM L-glutamine, 100 $\mu$M $\beta$-mecaptoethanol, and 4 ng/mL bFGF (Invitrogen, Carlsbad, CA). The media were changed everyday, and cells were passaged every 5 days. All cultures were monitored with hES cell undifferentiated markers staining against SSEA-3, SSEA-4, TRA-1-81, and TRA-1-60, as well as RT-PCR for Oct-4 and Nanog. Alkaline phosphatase staining kit and antibodies against TRA-1-81, TRA-1-60, and SSEA-3 were purchased from Chemicon (Temecula, CA). For AFM analysis, sterilized plastic slides ($1 \times 1$ cm$^2$) were cut out from cell culture dishes. The slides were coated with Matrigel (BD Biosciences, Franklin Lakes, NJ) for 2 h at 37 °C. Individual hES cell colonies with typical undifferentiated morphology were manually picked up from the feeder layer by a thin-tip pipet under a microscope and replated onto Matrigel-coated slides for feeder-free culture with MEF-conditioned medium plus freshly added 4 ng/mL bFGF.

**Immunofluorescent Staining.** hES cells were grown on feeder-free plastic slides in conditioned medium. The cells were fixed and permeabilized with cold methanol for 7 min at room temperature and incubated with 1% BSA in PBST for 1 h to block the nonspecific binding of antibodies. The cells were then incubated with primary antibodies in 1% BSA in PBST for 2 h at room temperature or 24 h at 4 °C. After three washes with PBS, the cells were incubated with secondary antibodies in 1% BSA for 1 h at room temperature in the dark. The nuclei were then stained with DAPI (Invitrogen, Eugene, OR) for 15 min. The following antibodies and dilutions were used: rabbit anti-Oct-4 (Abcam, Cambridge, MA), 1:100; mouse anti-E-cadherin (Zymed, Carlsbad, CA), 1:50; mouse anti-TRA-1-81 (Millipore, Billerica, MA), 1:50; Alexa Flour-488 or Alexa Flour-594 conjugated donkey antimouse or donkey antirabbit (Invitrogen, Carlsbad, CA), 1:200; NL493 conjugated donkey antigoat (R&D System, Minneapolis, MN), 1:200. The immunofluorescent staining was visualized with a Nikon TE-U 2000 fluorescence microscope.

**AFM Measurements and Data Analysis.** After 48 h feeder-free culture on a precut $1 \times 1$ cm$^2$ plastic slide, the cells were rinsed twice with PBS buffer. Cells were fixed by cold methanol for 7 min to avoid the migration of cell surface proteins during the steady-state analysis of protein distribution. PBS buffer (pH = 7.4) was used as the medium in all experiments.

AFM measurements were carried out at room temperature in a commercial liquid cell using a multimode Nanoscope IIIa AFM (Veeco Metrology, Santa Barbara, CA). $Si_3N_4$ tips at a thermal resonance frequency of 8−10 kHz were used in the study. The spring constant of the tips was 0.07 ± 0.01 N/m, as calibrated by using reference cantilevers with known spring constants.[21,28] AFM imaging was performed in fluid tapping mode using a bare tip; force volume imaging was performed in fluid contact mode using a functionalized tip.

**Scheme 1. Functionalization of AFM Probe by Antibody against TRA-1-81**

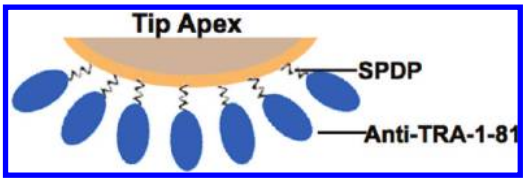


We functionalized TRA-1-81 antibody on an AFM tip using a cross-linker *N*-succinimidyl 3-(2-pyridyldithio)propionate (SPDP, Molecular Probes, Eugene, OR) as routinely performed in our lab,[21,22,29−32] as shown in Scheme 1. $Si_3N_4$ tips (Veeco) were coated with titanium (3 nm thickness) and gold (15 nm thickness) by a thermoevaporator (Denton Vacuum, Moorestown, NJ). After UV−ozone treatment using a tip cleaner (Bio-Force Nanosciences Inc., Ames, IA), the tips were immersed in a $1.64 \times 10^{-3}$ M SPDP solution in acetonitrile at room temperature under $N_2$ protection, generating a monolayer of SPDP on a tip via the thiol−gold linkage. The modified tips were then immersed in a solution of $10^{-6}$ M of antibody (in PBS of pH 7.4) overnight at room temperature under $N_2$ protection. The tips were thoroughly rinsed after each modification step to remove any unbound residues. According to the topographic images of gold-coated silicon wafer that functionalized by antibodies under the same conditions, antibodies were uniformly and densely distributed across the surface. The monolayer coverage was evaluated by the 8 ± 1 nm thick protein layer with respect to the bare substrate. Occasionally, physically adsorbed protein clusters were observed on the protein monolayer. The same surface feature is expected on antibody-functionalized AFM tips. Physically adsorbed proteins are less stable, hence easily detach from a tip. To warrant the consistency of antibody coverage on tips in all experiments, we chose to use the tips showing reproducible adhesion forces measured at the same sample location in multiple approaching and retraction cycles. This property is an indication of monolayer coverage of covalently bound antibodies. A gold-coated tip was also modified by oligoethylene glycol ($HSC_{11}$-$EG_6$, ProChimia, Gdansk, Poland) to evaluate the level of nonspecific interaction between the tip and a cell membrane surface.

When a functionalized tip scanned a cell surface, a force spectrum was recorded at each pixel upon the tip approach and retraction. The z-scan rate of the measurements was 1.33 Hz, and the z-ramp size was 2 $\mu$m. Typically, a strong adhesion peak in the retraction curve reveals the unbinding of antigen−antibody specific interaction, thus reports the presence of the membrane protein. A total of $32 \times 32 = 1024$ force curves were collected (regardless of the scan size) to construct a force volume (FV) image, in which the contrast was indicated by the maximum adhesion force measured at each pixel. The original force−distance curves were then converted to force−extension curves, where the extension is the difference between the z-position and the z-deflection. The separation work at each pixel was calculated from the area under the retraction curve by applying trapezoidal integration. An affinity map is constructed based on the separation work per pixel using a Matlab-based program developed in-house (see Supporting Information) and illustrates the distribution of TRA-1-81 on the cell membrane.

## RESULTS

**TRA-1-81 Expression on a hES Cell Colony.** TRA-1-81 antigen is a keratan sulfate proteoglycan,[33,34] which is expressed

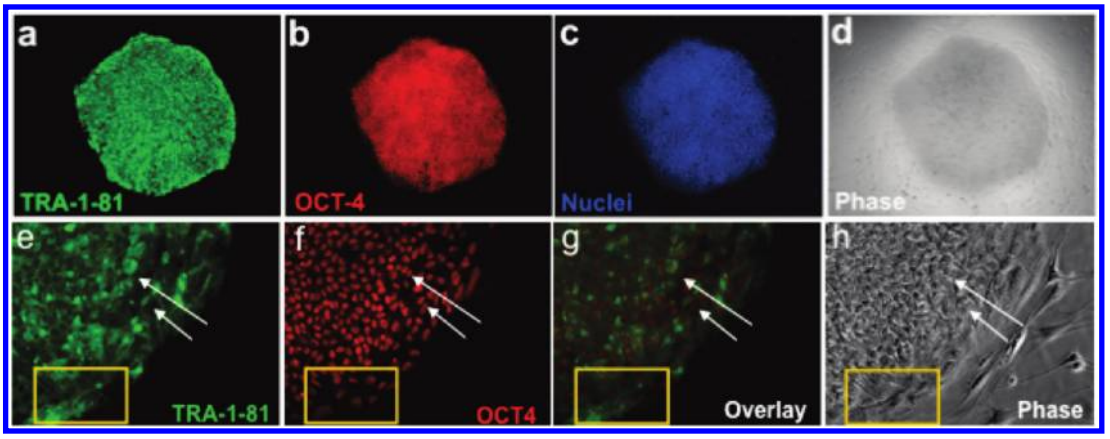


**Figure 1.** Immunofluorescence analysis of hES cells. (a−c) Immunostaining of an undifferentiated hES cell colony against TRA-1−81 (a), Oct-4 (b), and nuclei (c). (d) Phase image of the same colony as shown in a−c. (e, f) Enlarged images showing a portion of a hES cell colony staining against TRA-1-81 (e), Oct-4 (f), and the overlay of panels e and f. (g) Phase image of the same area shown in panels e and f. Arrow pointed round-shaped cells in panels e−h show Oct-4 positive and TRA-1-81 low to negative expression. The rectangular box highlights cells departing from the colony and expressing TRA-1-81 and Oct-4 at variable levels.

in undifferentiated hES cells and dramatically down-regulated in differentiated cells. hES cells proliferate in colonies with well-defined boundaries. Cells within a colony are commonly round in shape with a dimension of 10−20 $\mu$m in diameter. Figure 1a−d shows the immunofluorescent images of a typical hES cell colony containing about 2500 cells. In general, cells within a colony express hES cell markers OCT4 and TRA-1-81 at a high level, attesting to their undifferentiated status. At the boundary of a cell colony as shown in Figure 1e−h (highlighted by the rectangular box), cells departing from a colony spread to occupy a larger area per cell and display various shapes distinct from the round-shaped undifferentiated cells. Apparently, these cells are committed to differentiation. However, the cells are both OCT4-positive and TRA-1-81-positive; immunostaining can hardly discriminate the difference in marker protein expression level of these cells from that of the cells at the center of a colony. On the other hand, we occasionally observed some OCT4-positive, round-shaped cells expressing TRA-1-81 at a low or negligible level (arrow-pointed). This is consistent with the speculation that a side-population of cells exists within a healthy hES cell colony. Although the function of TRA-1-81 is uncertain, the association and the expression level of TRA-1-81 are closely relevant to hES cell development. Since heterogeneity exists among individual cells, it is essential to acquire quantitative information of protein expression at the single cell level. This motivated the AFM work as delineated below.

**Affinity Mapping against TRA-1-81.** We performed affinity mapping to probe the association and the distribution of cell surface protein TRA-1-81 at the single cell level. AFM tips modified with the antibody against TRA-1-81 were employed. Figure 2a shows the 3D height image of a whole cell at 512 pixels per line. An area of 8 × 8 $\mu$m$^2$ (highlighted by the square box) was chosen to collect the height image (Figure 2c) and the FV image (Figure 2d) simultaneously at 32 pixels per line. Figure 2b shows the typical force curves collected at the highlighted pixels in Figure 2c,d. The coloration of the FV image is scaled on the basis of the maximum adhesion force measured at each pixel. When examining the force curves, we observed that a retraction curve frequently showed a steep slope followed by a slow decrease before the tip jumped from the surface; the adhesion peaks in different pixels varied in both shape and separation

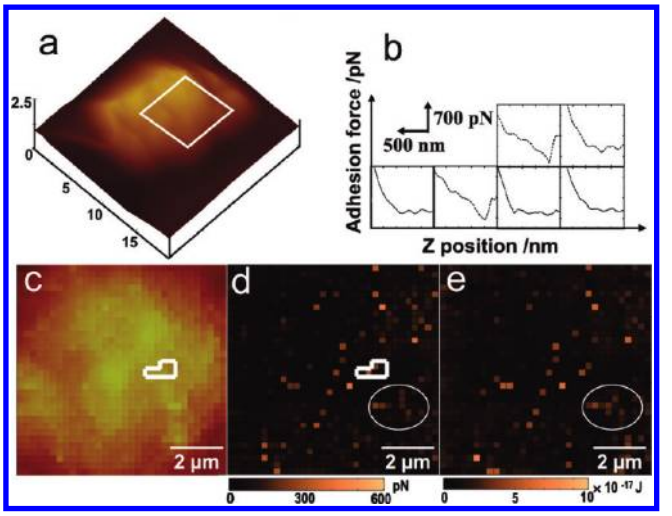


**Figure 2.** AFM measurements on a hES cell. (a) 3D height image of a hES cell captured at 512 pixels per line at a lateral scale of 20 × 20 $\mu$m$^2$. (b) Force curves collected at the highlighted pixels in panels c and d. (c) 8 × 8 $\mu$m$^2$ height image collected at 32 pixels per line at the framed area in panel a by an anti-TRA-1-81 modified tip. (d) 8 × 8 $\mu$m$^2$ force volume image collected simultaneously with panel c. (e) 8 × 8 $\mu$m$^2$ affinity map reproduced by evaluating the separation work based on the force curve per pixel in panel d. The circled region illustrates the disparity between the force volume image (d) and the affinity map (e).

distance. Multiple peaks appeared in some pixels. Therefore, an FV image, the contrast of which is based on the maximum adhesive force, does not provide accurate and complete information of protein expression and local distribution. We generated separation work-based affinity maps as shown in Figure 2e (at the same 8 × 8 $\mu$m$^2$ area as of Figure 2d). The separation work is calculated based on the shape and intensity of a force curve, which carries more comprehensive information of the specific binding event(s) at a pixel. Variation in map contrast was frequently found between panels d and e of Figure 2 (e.g., in the circled region). In later sections, analysis of protein abundance was carried out on the basis of separation work per pixel.

To examine the reproducibility of affinity maps, we sequentially collected affinity maps at a high-force region (framed area)


dx.doi.org/10.1021/la200817b |*Langmuir* 2011, 27, 8294–8301

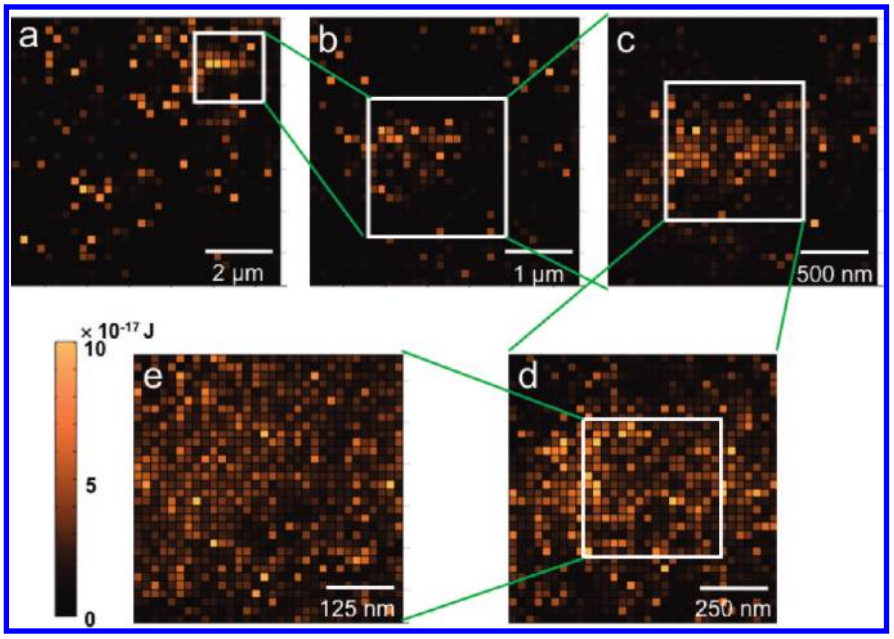


**Figure 3.** Affinity maps reconstructed from force volume images collected sequentially at scales of 8 × 8 $\mu m^2$ (a), 4 × 4 $\mu m^2$ (b), 2 × 2 $\mu m^2$ (c), 1 × 1 $\mu m^2$ (d), and 500 × 500 $nm^2$ (e). The framed areas highlight the same high-force region that was examined subsequently at smaller scales.

at scales of 8 × 8 $\mu m^2$, 4 × 4 $\mu m^2$, 2 × 2 $\mu m^2$, 1 × 1 $\mu m^2$, and 500 × 500 $nm^2$ as shown in Figure 3. The same contrast was detected at the same local region in all maps, suggesting that affinity mapping is a reliable method to investigate protein distributions. In the large-scale maps (Figure 3a−c), we found that the distribution of TRA-1-81 was heterogeneous, characterized by largely segregated protein aggregates in bright contrast. This unique heterogeneous distribution of TRA-1-81 was observed on all undifferentiated cells investigated (more than 10 cells). In contrast, homogeneous distribution of TRA-1-81 is characteristic for initially differentiated cells[21] accompanied by a decline in the protein expression level.

**Local Force Analysis.** Common and distinct force curves were observed in the maps at different scales. For instance, the four pixels highlighted in the 8 × 8 $\mu m^2$ map (Figure 4a) match the sixteen pixels in location highlighted in the 4 × 4 $\mu m^2$ map (Figure 4c). Figure 4, panels b and d, illustrates the adhesion force curves at the highlighted pixels. The adhesion forces measured at pixels i, ii, iii, and iv in the two maps are similar in both shape and magnitude. It suggests that the pairs of pixels in the two maps mark the same antigens. While the four pixels in Figure 4a are all identified in Figure 4c, other pixels in Figure 4c mark additional antigens registered at the local region. The results imply that TRA-1-81 antigens were incompletely reported in an 8 × 8 $\mu m^2$ affinity map and were better resolved in a 4 × 4 $\mu m^2$ affinity map.

A decrease in the mapping size does not warrant a better resolution of protein distribution and association. Figure 4e shows the 500 × 500 $nm^2$ affinity map, and the force curves of the highlighted pixels are shown in Figure 4f. At the local region n, as many as six duplicated force curves were observed. It implies that the same proteins were repeatedly registered at the multiple pixels. Similar force curves were recorded at regions m, p, and q. The result suggests that TRA-1-81 antigens were overaddressed in a 500 × 500 $nm^2$ affinity map. A match between the tip size and the pixel size is imperative to accurately report the protein distribution and association. It also defines the lateral resolution of an affinity map.

**Histograms and Nonspecific Interaction.** Figures 5 and 6 show the histograms which summarize the frequency of observing a specific amount of separation work in the 8 × 8 $\mu m^2$ to 500 × 500 $nm^2$ affinity maps in Figure 3. The histograms can provide quantitative information only if the level of nonspecific interaction is identified. Because the affinity maps in Figure 3 were sequentially collected at a high-force region, the 500 × 500 $nm^2$ map marked TRA-1-81 antigens at every pixel of the map according to the force curves and the map contrast. The cell surface was relatively smooth at this small scale according to our height images, and the high local density of TRA-1-81 antigens excluded other cell surface species at the local region. Hence, the separation work detected in the small-scale affinity map is attributed to the specific antigen−antibody interaction; the minimum separation work of 6 × $10^{-18}$ J (see Figure 6d) defines the level of nonspecific interaction. The frequencies of observing separation work less than 6 × $10^{-18}$ J were 4%, 27%, 50%, and 52% at scan scales of 1 × 1 $\mu m^2$, 2 × 2 $\mu m^2$, 4 × 4 $\mu m^2$, and 8 × 8 $\mu m^2$, respectively. This suggests that the frequency of observing nonspecific interaction is significantly higher in a large-scale affinity map, most likely due to the complexity of surface features on a cell membrane.

Though nonspecific interaction can be largely neglected in small-scale affinity maps, with the current experimental setting, 4 × 4 $\mu m^2$ affinity maps are suitable for quantitative studies when the probe resolution is taken into consideration (see Discussion). To corroborate the level of nonspecific interaction at this scale, we carried out control experiments. We applied a PEG-modified tip to collect 4 × 4 $\mu m^2$ affinity maps. On the basis of the absence of antibody on the tip and the cell-resistant nature of PEG, any detected separation work is ascribed to nonspecific interactions, arising from tip convolution, cell surface roughness, and the weak interaction of PEG with various cell-surface species.[22] As shown in Figure 5b (blue columns), the most probable separation work

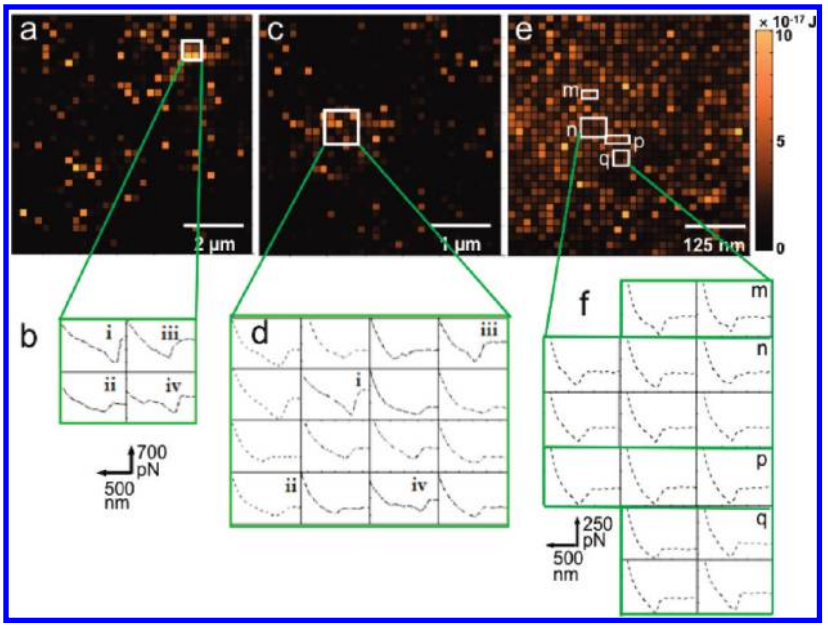


**Figure 4.** Comparison of retraction curves collected on affinity maps at different scales. (b, d, f) Force curves at the highlighted pixels in the $8 \times 8\ \mu m^2$ (a), $4 \times 4\ \mu m^2$ (c), and $500 \times 500\ nm^2$ (e) affinity maps, respectively. The highlighted four pixels in the $8 \times 8\ \mu m^2$ map match the sixteen pixels in location in the $4 \times 4\ \mu m^2$ map.

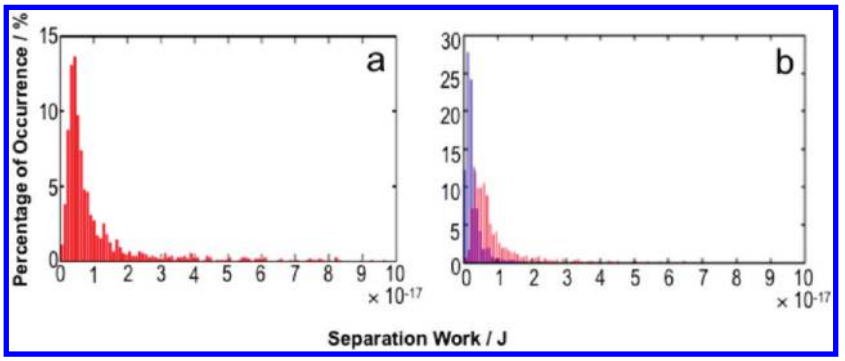


**Figure 5.** Probability histograms of the separation work summarized from the $8 \times 8\ \mu m^2$ (a) and $4 \times 4\ \mu m^2$ (b, red columns) affinity maps in Figure 3a, b. The blue columns in panel b represent the probability histogram summarized from three $4 \times 4\ \mu m^2$ affinity maps collected by a PEG-modified tip on undifferentiated cells (control experiment).

appears at $1 \times 10^{-18}$ J, and 90% of the measured separation work is lower than $6 \times 10^{-18}$ J. We also incubated the cells in culture media containing 1% BSA for 1 h, followed by incubation in media containing 10 μg/mL of antibody against TRA-1-81 for 2.5 h to abolish the antigens on the cell membrane. When an antibody-modified tip scanned the surface, we found that adhesions were largely abrogated with the most probable separation work measured at $2 \times 10^{-18}$ J, and 86% of the separation work below $6 \times 10^{-18}$ J. These attest that the $6 \times 10^{-18}$ J separation work is a reasonable cutoff to define the level of nonspecific interaction.

Because of the low level of nonspecific interaction, a small-scale affinity map facilitates the derivation of the single-pair antigen−antibody interaction (Figure 6). Gaussian fitting was first carried out for affinity maps at $1 \times 1\ \mu m^2$ and $500 \times 500\ nm^2$. We identified six peaks at 1.12, 2.19, 3.40, 4.47, 5.54, 6.62 $\times 10^{-17}$ J in Figure 6c, and 1.26, 2.16, 3.29, 4.42, 5.55, 6.57 $\times 10^{-17}$ J in Figure 6d, which appear to be integer multiples of a quanta unit $1.1 \times 10^{-17}$ J. The same trend was found for larger-scale affinity maps. Thus, $1.1 \times 10^{-17}$ J is estimated to be the separation work of a single-pair antigen−antibody interaction, consistent with the report by Ikai et al.[35] With the same set of data, we also estimated the strength of a single-pair antigen−antibody interaction at 110 pN level using the maximum adhesion force-based method. The inset of Figure 6d shows a typical force curve of the single-pair specific recognition event. The maximum adhesion force was measured at 122 pN, and the separation work was $9.6 \times 10^{-18}$ J. The results imply a reasonable agreement within the two methods in quantifying the single-pair specific interaction; however, the separation work-based method is superior, as it avoids the omission of proteins in multibinding events. The identification of the separation work between a single pair antigen−antibody and the level of nonspecific interaction laid the groundwork for quantifying protein densities on single cells.

## DISCUSSION

The current study establishes a versatile method for examining membrane proteins quantitatively. This was achieved by using an

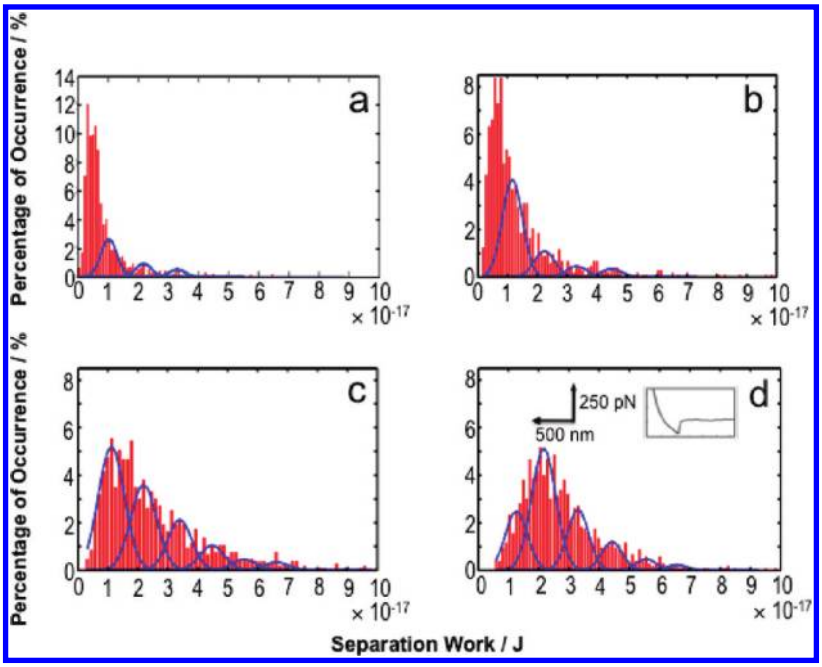


**Figure 6.** Comparison of the probability histograms of separation work at different scan scales: (a) $4 \times 4\ \mu m^2$, (b) $2 \times 2\ \mu m^2$, (c) $1 \times 1\ \mu m^2$, and (d) $500 \times 500\ nm^2$. The histograms were fitted with a Gaussian. On the basis of the fitted peaks, the strength of a single-pair antigen−antibody interaction was evaluated at $1.1 \times 10^{-17}$ J. The inset of panel d is a typical force curve showing the single-pair binding event.

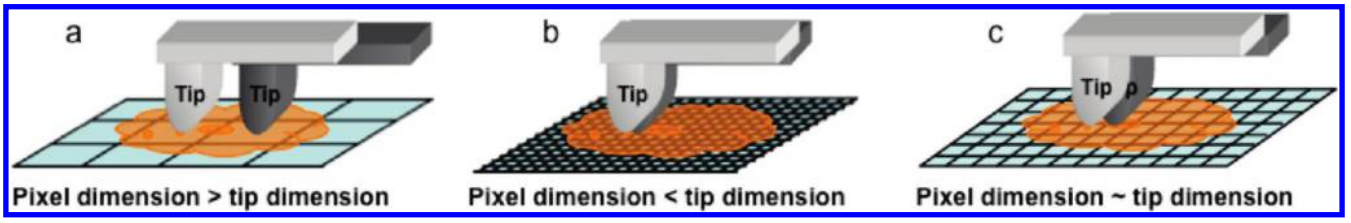


**Figure 7.** Schematic illustration of probe resolution in affinity mapping. An AFM probe addresses proteins on a cell membrane when the pixel dimension is greater than (a), less than (b), or approximately the same as (c) the tip dimension. The probe resolution is limited by the probe dimension.

antibody-modified AFM tip to locate the antigen pixel by pixel across the membrane surface, and the report of the membrane proteins was based on the separation work above the level of nonspecific interaction.

**Probe Resolution.** For accurate quantification, each protein must be counted only once. As illustrated in Figure 7, when the tip dimension is less than the pixel size (Figure 7a), some membrane proteins may be omitted; when the tip dimension is greater than the pixel size (Figure 7b), some membrane proteins may be overcounted. Only when the tip dimension and the pixel size are approximately the same (Figure 7c) can the proteins on the cell membrane be adequately and precisely addressed. The experimental evidence is shown in Figure 4. Even when the probe size matches the pixel size, proteins at the interface of adjacent pixels may cause repeat-count of proteins. This is especially true when these proteins are closely associated. Analysis of smaller scale affinity maps sequentially collected at the same local region is expected to further resolve the protein association; examination of affinity maps acquired with different scanning angles and at the same area will permit more accurate protein quantification. Regular tip shape and well-defined contact area are also expected to improve the accuracy in protein quantification. This investigation has been undertaken in our research group.

According to the SEM images of gold-coated probes, the radius of the tip apex was about 35 nm. Taking account of the dimension of a cross-linker SPDP (~0.7 nm in length) and an antibody IgM (24 nm in diameter),[36−38] we estimate the diameter of the tip contact area as ~120 nm, which matches approximately one pixel (125 nm) in a $4 \times 4\ \mu m^2$ affinity map. Therefore, a $4 \times 4\ \mu m^2$ affinity map is competent for analyzing the protein distribution and quantifying the protein abundance. This scale may vary in other studies and should be adjusted based on the dimensions of the contact region and the ligand. The protein distribution was resolved at the single pixel level, i.e., an area of $125 \times 125\ nm^2$ in a $4 \times 4\ \mu m^2$ affinity map in our case. The maximum separation work measured was $9.83 \times 10^{-17}$ J, implying that at least 9 effective binding sites were available at the contact area of the tip (the tip apex can accommodate a maximum of 11 antibodies). The improvement of the lateral resolution can be made by reducing the dimension of the modified probe, which can be achieved by either reducing the dimension of the tip apex or modifying the antibodies within a constrained small area of a tip. Because a sharp tip can easily indent and penetrate a cell membrane and complicate adhesion force measurements, the latter is a better choice. While the SPDP-linked antibody was utilized to probe TRA-1-81 on the


dx.doi.org/10.1021/la200817b |*Langmuir* 2011, 27, 8294–8301

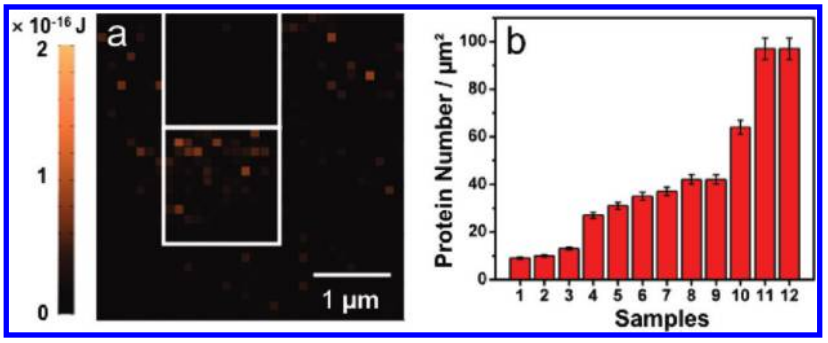


**Figure 8.** Local abundance of TRA-1-81 on hES cells. (a) Distinct protein expression levels quantified on the 4 × 4 $\mu m^2$ affinity map. The protein density was evaluated at 15 ± 1/$\mu m^2$ (upper square) and 192 ± 9/$\mu m^2$ (lower square), respectively. (b) Comparison of protein density on 12 different cells selected at the center of hES cell colonies.

cell membrane, the use of a flexible spacer in the cross-linker and the dilution of antibody on the tip are expected to reduce the nonspecific interaction and the steric restriction on the recognition events.[39−41] These will be pursued in our future studies.

**Evaluation of Protein Local Abundance.** On the basis of the single-pair antigen−antibody interaction of 1.1 × $10^{-17}$J, we quantified the local protein density by integrating the areas below the fitting curves in the histogram of a selected affinity map (see Figure 6). The protein density on the entire 4 × 4 $\mu m^2$ map was averaged at 35 ± 2/$\mu m^2$, whereas the protein densities were 192 ± 9/$\mu m^2$ and 15 ± 1/$\mu m^2$, respectively, at the highlighted bright-contrast and dark-contrast local regions in Figure 8a. These indicate the heterogeneous distribution of TRA-1-81. The large-scale affinity maps in Figure 3 show that the high separation work regions are localized and apparently segregated by low separation work regions, further supporting the heterogeneous distribution of TRA-1-81 on the hES cells.

For comparison, we also collected 4 × 4 $\mu m^2$ affinity maps against another membrane protein, E-cadherin (maps not shown). When we equally divided the map into four regions, E-cadherin density was estimated at 327 ± 15, 374 ± 17, 354 ± 24, and 381 ± 17 proteins/$\mu m^2$, respectively, indicating homogeneous distribution of E-cadherin on the cell membrane with a much higher protein density. Taken together, the affinity mapping method is powerful in quantifying protein density and probing heterogeneity of protein distribution at the subcellular level. The localization and aggregated distribution of TRA-1-81 are characteristic in undifferentiated hES cells, in contrast to the random distribution of the occasionally observed antigens on differentiated cells.[21] The heterogeneous distribution pattern of TRA-1-81 may be used as a physical marker to identify hES cell status.

Note that the quantification was based on separation work. Separation work reflects the dynamics of a specific binding event and thus is a better measure of protein abundance on a surface as complex as a cell membrane. As a comparison, we evaluated the protein local abundance on the basis of maximum adhesion force on the same 4 × 4 $\mu m^2$ affinity map in Figure 8a. The average protein density was at 20 ± 2/$\mu m^2$, and the protein densities were 105 ± 7/$\mu m^2$ and 11 ± 1/$\mu m^2$, respectively, at the highlighted bright-contrast and dark-contrast local regions. The disparity results from the exclusion of some of the binding features in the maximum adhesion force measurements. Though control experiments were performed to define the level of nonspecific interaction, it is concerned that occasionally high separation work may reflect the high-level of nonspecific cell adhesion and may cause the overcount of proteins. We envision that the combination of the data derived from maximum force and separation work will lead to more accurate protein quantification. In reference to other AFM studies, we applied Gaussian distribution in fitting the histograms to achieve protein quantification. More comprehensive fitting methods are expected to improve the accuracy of quantification.

In the study of multiple cells, we found that TRA-1-81 expression level differs remarkably on distinct cells, consistent with the qualitative characterization by immunofluorescent imaging (Figure 1). Figure 8b summarizes the average protein density sampled on 12 different cells selected at the center of hES cell colonies. While the majority of the cells expressed TRA-1-81 at a level of 30−45 proteins/$\mu m^2$, fluctuation was observed, ranging from 9 ± 1 to 97 ± 5 proteins/$\mu m^2$. This result implies that heterogeneity is present in well-defined undifferentiated cell colonies. This coincides with previous observations. For instance, Mantel et al. reported a small population of TRA-1-60 negative cells in an undifferentiated cell colony.[42] Similarly, Stewart et al.[43] identified both SSEA-3 positive and SSEA-3 negative cells by screening and isolating single cells within an undifferentiated cell colony using flow cytometry. Both cell types were found to initiate pluripotent hES cell cultures; however, they possessed distinct cell-cycle properties, clonogenic capacity, and expression of ES cell transcription factors.[43] It was suggested that heterogeneous population within a stem cell colony is necessary for coordinating self-renewal of undifferentiated cells;[43] the fluctuations and their time evolutions may play a functional role in introducing the cell variability that is observed during development.[14,20,44] The variation of TRA-1-81 expression level within a colony of undifferentiated cells is likely a similar requirement for hES cell self-renewal and further development.

## CONCLUSION

We established an affinity mapping method based on the separation work to illustrate and evaluate the membrane protein distribution and local abundance on single cells. Sequential affinity maps acquired in the same region demonstrate the reproducibility and reliability of information derived from this method. The level of nonspecific interaction is remarkably lower on small-scale affinity maps. This facilitates the determination of the strength of single-pair antigen−antibody interaction. However, the choice of a proper mapping scale is imperative to warrant the accurate and adequate evaluation of protein abundance. Applying

this method, we probed the distribution and the local abundance of TRA-1-81 antigen on hES cells. We revealed the heterogeneity in TRA-1-81 expression at both the subcellular level and the cell colony level, which are likely attributed to intrinsic and extrinsic origins of fluctuations necessary for the stem cell proliferation and differentiation.

The affinity mapping method is versatile in studies of various types of cells in their native states. A singular advantage of the AFM approach is that membrane proteins can be quantitatively analyzed with spatial resolution at subcellular and single cell levels. The quantitative method is more sensitive than methods based on optical imaging; higher sensitivity is expected by reducing the probe size. The method provides a potential platform to unveil the regulatory relationships of proteins and genes within a cell or in neighboring cells in a cell community at the earliest phases of cell development and differentiation. A significant drawback of the method at the current stage, however, is the slow process of force measurement, which hinders its throughput in dynamic studies of cells at different statuses and in various stages during the development. The recent advancement in fast scanning AFM is expected to provide a promising solution to this issue.

## ■ ASSOCIATED CONTENT

**Supporting Information.** Matlab code for generating affinity maps and calculating protein numbers. This material is available free of charge via the Internet at http://pubs.acs.org.

## ■ AUTHOR INFORMATION

### Corresponding Author

*E-mail: wangr@iit.edu. Tel: 312-567-3121. Fax: 312-567-3494.

## ■ ACKNOWLEDGMENT

This research was supported by NIH (R01 NS047719) and a seed grant from the Pritzker Institute of Biomedical Science and Engineering at IIT.

## ■ REFERENCES

(1) Bauwens, C. L.; Peerani, R.; Niebruegge, S.; Woodhouse, K. A.; Kumacheva, E.; Husain, M.; Zandstra, P. W. *Stem Cells* **2008**, *26*, 2300.
(2) Reya, T.; Clevers, H. *Nature* **2005**, *434*, 843.
(3) Bendall, S. C.; Stewart, M. H.; Menendez, P.; George, D.; Vijayaragavan, K.; Werbowetski-Ogilvie, T.; Ramos-Mejia, V.; Rouleau, A.; Yang, J.; Bosse, M.; Lajoie, G.; Bhatia, M. *Nature* **2007**, *448*, 1015.
(4) Watt, F. M.; Hogan, B. L. M. *Science* **2000**, *287*, 1427.
(5) Shackleton, M.; Vaillant, F. O.; Simpson, K. J.; Stingl, J.; Smyth, G. K.; Asselin-Labat, M.-L.; Wu, L.; Lindeman, G. J.; Visvader, J. E. *Nature* **2006**, *439*, 84.
(6) Prince, M. E.; Sivanandan, R.; Kaczorowski, A.; Wolf, G. T.; Kaplan, M. J.; Dalerba, P.; Weissman, I. L.; Clarke, M. F.; Ailles, L. E. *Proc. Natl. Acad. Sci. U.S.A.* **2007**, *104*, 973.
(7) Stephens, D. J.; Allan, V. J. *Science* **2003**, *300*, 82.
(8) Liou, J.; Fivaz, M.; Inoue, T.; Meyer, T. *Proc. Natl. Acad. Sci. U.S.A.* **2007**, *104*, 9301.
(9) Newman, J. R. S.; Ghaemmaghami, S.; Ihmels, J.; Breslow, D. K.; Noble, M.; DeRisi, J. L.; Weissman, J. S. *Nature* **2006**, *441*, 840.
(10) Bar-Even, A.; Paulsson, J.; Maheshri, N.; Carmi, M.; O'Shea, E.; Pilpel, Y.; Barkai, N. *Nat. Genet.* **2006**, *38*, 636.
(11) Zhong, J. F.; Feng, Y.; Taylor, C. R. *Curr. Med. Chem.* **2008**, *15*, 2897.
(12) Ryley, J.; Pereira-Smith, O. M. *Yeast* **2006**, *23*, 1065.
(13) Kobel, S.; Lutolf, M. P. *BioTechniques* **2010**, *48*, 14.
(14) Zhong, J. F.; Chen, Y.; Marcus, J. S.; Scherer, A.; Quake, S. R.; Taylor, C. R.; Weiner, L. P. *Lab Chip* **2008**, *8*, 68.
(15) Larson, D. R.; Singer, R. H.; Zenklusen, D. *Trends Cell Biol.* **2009**, *19*, 630.
(16) Emmert-Buck, M. R.; Bonner, R. F.; Smith, P. D.; Chuaqui, R. F.; Zhuang, Z.; Goldstein, S. R.; Weiss, R. A.; Liotta, L. A. *Science* **1996**, *274*, 998.
(17) Wang, K.; Lau, T. Y.; Morales, M.; Mont, E. K.; Straus, S. E. *J. Virol.* **2005**, *79*, 14079.
(18) Chiang, L. W. *J. Chromatogr. A* **1998**, *806*, 209.
(19) Audinat, E.; Lambolez, B.; Rossier, J. *Neurochem. Int.* **1996**, *28*, 119.
(20) Gibson, J. D.; Jakuba, C. M.; Boucher, N.; Holbrook, K. A.; Carter, M. G.; Nelson, C. E. *Integr. Biol.* **2009**, *1*, 540.
(21) Qiu, D.; Xiang, J.; Li, Z.; Krishnamoorthy, A.; Chen, L.; Wang, R. *Biochem. Biophys. Res. Commun.* **2008**, *369*, 735.
(22) Li, Z.; Qiu, D.; Sridharan, I.; Qian, X.; Zhang, H.; Zhang, C.; Wang, R. *J. Phys. Chem. B* **2010**, *114*, 2894.
(23) Liu, S.; Wang, Y. *Scanning* **2010**, *32*, 61.
(24) Allison, D. P.; Mortensen, N. P.; Sullivan, C. J.; Doktycz, M. J. *Wiley Interdiscip. Rev. Nanomed. Nanobiotechnol.* **2010**, *2*, 618.
(25) Junker, J. P.; Rief, M. *Proc. Natl. Acad. Sci. U.S.A.* **2009**, *106*, 14361.
(26) Bhushan, B.; Fuchs, H. *Applied scanning probe methods III: Characterization*; Springer-Verlag: Berlin, 2006.
(27) Stroh, C.; Wang, H.; Bash, R.; Ashcroft, B.; Nelson, J.; Gruber, H.; Lohr, D.; Lindsay, S. M.; Hinterdorfer, P. *Proc. Natl. Acad. Sci. U.S.A.* **2004**, *101*, 12503.
(28) Tortonese, M.; Kirk, M. In *Micromachining and Imaging*, 1st ed.; SPIE: San Jose, CA, 1997; Vol. 3009, p 53.
(29) Tang, Q.; Zhang, Y.; Chen, L.; Yan, F.; Wang, R. *Nanotechnology* **2005**, *16*, 7.
(30) Yan, F.; Chen, L.; Tang, Q.; Wang, R. *Bioconjugate Chem.* **2004**, *15*, 1030.
(31) Reddy, C. V. G.; Malinowska, K.; Menhart, N.; Wang, R. *Biochim. Biophys. Acta. Biomembr.* **2004**, *1667*, 15.
(32) Vengasandra, S.; Sethumadhavan, G.; Yan, F.; Wang, R. *Langmuir* **2003**, *19*, 10940.
(33) Badcock, G.; Pigott, C.; Goepel, J.; Andrews, P. W. *Cancer Res.* **1999**, *59*, 4715.
(34) Wolf, D. P.; Kuo, H.-C.; Pau, K.-Y. F.; Lester, L. *Biol. Reprod.* **2004**, *71*, 1766.
(35) Hyonchol, K.; Arakawa, H.; Osada, T.; Ikai, A. *Colloids Surf., B* **2002**, *25*, 33.
(36) Bakoush, O.; Tencer, J.; Tapia, J.; Rippe, B.; Torffvit, O. *Kidney Int.* **2002**, *61*, 203.
(37) Roberts, C. J.; Davies, M. C.; Tendler, S. J. B.; Williams, P. M.; Davies, J.; Dawkes, A. C.; Yearwood, G. D. L.; Edwards, J. C. *Ultramicroscopy* **1996**, *62*, 149.
(38) Czajkowsky, D. M.; Shao, Z. *Proc. Natl. Acad. Sci. U.S.A.* **2009**, *106*, 14960.
(39) Ebner, A.; Wildling, L.; Kamruzzahan, A. S. M.; Rankl, C.; Wruss, J.; Hahn, C. D.; Hölzl, M.; Zhu, R.; Kienberger, F.; Blaas, D.; Hinterdorfer, P.; Gruber, H. J. *Bioconjugate Chem.* **2007**, *18*, 1176.
(40) Barattin, R.; Voyer, N. *Chem. Commun.* **2008**, 1513.
(41) Kienberger, F.; Ebner, A.; Gruber, H. J.; Hinterdorfer, P. *Acc. Chem. Res.* **2005**, *39*, 29.
(42) Mantel, C.; Guo, Y.; Lee, M. R.; Kim, M.-K.; Han, M.-K.; Shibayama, H.; Fukuda, S.; Yoder, M. C.; Pelus, L. M.; Kim, K.-S.; Broxmeyer, H. E. *Blood* **2007**, *109*, 4518.
(43) Stewart, M. H.; Bosse, M.; Chadwick, K.; Menendez, P.; Bendall, S. C.; Bhatia, M. *Nat. Methods* **2006**, *3*, 807.
(44) Banerjee, B.; Balasubramanian, S.; Ananthakrishna, G.; Ramakrishnan, T. V.; Shivashankar, G. V. *Biophys. J.* **2004**, *86*, 3052.